

Contents lists available at ScienceDirect

Journal of Catalysis

journal homepage: www.elsevier.com/locate/jcat



A transient kinetic analysis of the evolution of a reducible metal oxide towards catalyzing nonoxidative alkanol dehydrogenation



Sadia Afrin, Praveen Bollini*

Department of Chemical and Biomolecular Engineering, University of Houston, 4722 Calhoun Road, Houston, TX 77004, USA

ARTICLE INFO

Article history: Received 4 April 2020 Revised 20 June 2020 Accepted 18 August 2020 Available online 28 August 2020

Keywords: Cerium oxide Ethanol dehydrogenation Oxidative dehydrogenation Oxygen vacancies

ABSTRACT

Quantitative analyses of four sets of aerobic/anaerobic ethanol conversion transients point to the evolution of a native high-surface-area cerium oxide surface that effects the reduction half of the ethanol oxidation turnover to catalyzing, exclusively, nonoxidative ethanol dehydrogenation upon complete surface reduction. Aerobic-anaerobic switches at 498 K lead to new steady state dehydrogenation rates, rather than termination of catalytic acetaldehyde formation. Concurrent termination of oxygen imbalances (reflecting ceria reduction) and induction periods (reflecting active site creation) in anaerobic experiments point to ethanol dehydrogenation turnovers owing their provenance to surface reduction. Implausibly high vacancy densities obtained from analysis of oxygen imbalances when using acetaldehyde and CO2 formation rates, unlike those obtained when using water and CO₂ formation rates, point to the catalytic origin of at least part of the acetaldehyde formed during both aerobic-anaerobic switches and anaerobic induction periods. Normalized water molar flow rates, used as a measure of the relative contributions of catalytic and stoichiometric routes to acetaldehyde formation, evince a transition from stoichiometric ethanol oxidation to catalytic ethanol dehydrogenation upon progressive surface reduction. Hightemperature hydrogen pretreatments can be used to manipulate both the initial contribution of ethanol dehydrogenation to overall acetaldehyde formation as well as the fractional surface reduction that ethanol, rather than molecular hydrogen, effectuates. Alpha hydrogen-free titrants such as phenol, on the other hand, can be used to titrate sites contributing to catalytic alkanol dehydrogenation without altering the prevalence of stoichiometric routes responsible for site creation in the first place. The combination of transient experiments used herein capture, with clarity, the evolution in catalytic function of highsurface-area cerium oxide toward ethanol upon progressive reduction that originates from its stoichiometric conversion over a native, fully oxidized surface. Not unimportantly, the results also point to an avenue for the water-free synthesis of alkanals over reducible metal oxides.

© 2020 Elsevier Inc. All rights reserved.

1. Introduction

Cerium oxide—the most abundant rare-earth oxide in the earth's crust [1]—has been studied extensively as a catalytic material [2–8], and has also been applied commercially as an oxygen storage component in three-way catalyst systems for the treatment of automotive exhaust streams [9–12]. Key to ceria's catalytic and oxygen storage properties is its propensity to undergo rapid reduction—oxidation cycles in response to exposure to sub- and overstoichiometric amounts of oxygen, respectively [4,9,10]; its propensity to reversibly generate oxygen vacancies, combined with the significant body of existing work focused on examining the same, make it an ideal candidate to elucidate and clarify

oxygen vacancy catalytic function, and to compare and contrast molecular phenomena prevailing over reduced and oxidized surfaces.

The reactivity of alkanols, especially ethanol, has been used extensively for the purposes of deciphering active site requirements and unraveling operative reaction mechanisms over metal oxide surfaces [13–22]. Specifically, dehydration kinetics can provide insights into the nature and density of active sites effectuating acid-catalyzed turnovers [23,24], while inquiries into partial alkanol oxidation can provide analogous assessments of sites mediating redox turnovers [25,26]. Partial alkanol oxidation over transition metal oxides has been proposed to occur through Mars-van Krevelen redox cycles in which O–H and C–H bond cleavage and subsequent desorption of water constitute the reduction half of the cycle, and kinetically irrelevant reoxidation steps comprise the oxidation half of the cycle [27,28]. Existing

^{*} Corresponding author.

E-mail address: ppbollini@uh.edu (P. Bollini).

interpretations of catalytic data assume that vacancies created upon loss of lattice oxygen are reoxidized by gas-phase oxygen, but not directly involved in C-H or O-H bond cleavage steps, which instead occur exclusively over the reoxidized surface—an interpretation reinforced by the lack of catalytic alkanol dehydrogenation over substoichiometric supported Ru₂O catalysts [27] or vacancycontaining supported Group V-VI metal oxides [29]. Vacancymediated catalytic nonoxidative alkanol and alkane dehydrogenation, on the other hand, have in fact been proposed in the literature [30–32], thereby at the very least rendering plausible contributions from both oxidative and dehydrogenative routes under select sets of reaction conditions. Existing evidence for the prevalence of Mars-van Krevelen cycles that create oxygen vacancies in the reduction half of the cycle, combined with the plausibility of catalytic dehydrogenation occurring over reduced surfaces created during those reduction half cycles, led us to ask the question: Can the surface of a reducible metal oxide, under anaerobic conditions, transition from effecting exclusively the reduction half of the alkanol oxidation cycle when fully oxidized, to catalyzing dehydrogenation when fully reduced?

We choose, to this end, ethanol conversion over ceria surfaces, in part motivated by the existence of a temperature regime in which the lack of bulk oxygen mobility may preclude complications in data interpretation arising from bulk oxygen vacancy creation [6,10,33-35]. As shown in Section 3, such isolation of reduction exclusively to the cerium oxide surface ends up being key to demonstrating, with sufficient clarity, the evolution in catalytic function of the oxide surface upon progressive reduction. Also, crucially, using ethanol as a probe molecule allows operation in a low-temperature regime in which oxidation and dehydrogenation predominate over alkanol dehydration and alkanal condensation under both aerobic [5,36] and anaerobic conditions (Fig. S5, Supporting Information), thereby rendering unnecessary the deconvolution of effects of surface reduction on redox and acid catalysis. Several groups have identified reduced ceria surfaces as having a greater propensity than oxidized ones to produce molecular hydrogen when exposed to C_1 – C_3 alkanols. For example, Yee et al. noted smaller fractions of unreacted ethanol when temperature-programmed desorption was carried out on ceria reduced at 773 K, rather than unreduced ceria [34]. Whereas in the case of unreduced ceria two separate, concurrent peaks for ethanol and ethanal were measured, the high-temperature peak for reduced ceria was found to be composed exclusively of ethanal. Vohs and co-workers [37] and Mullins et al. [38] noted that while formaldehyde and water were the main products detected on oxidized ceria thin films, CO and H₂ were the main products observed in postreduction methanol TPD profiles. H₂:H₂O ratios were found to increase with the degree of ceria reduction in both these studies, as well as other reports in which C₁-C₃ alkanol TPD was carried out over (111) films [39] and methanol TPD was carried out over (100) films [40]. These studies point, albeit vaguely, to the occurrence of alkanol dehydrogenation over reduced ceria surfaces, with their contribution over oxidized surfaces remaining ambiguous at best. Complications arising from both stoichiometric and catalytic contributions in TPD runs exacerbate this ambiguity, making it even more challenging to interpret differences in catalytic function over oxidized and reduced surfaces. Additionally, although these studies evaluate the effect of oxide prereduction on surface reactivity, they do not, in most cases, explicitly consider the effect of reduction that could occur directly as a result of C1-C3 alkanol reactivity.

In contrast with these prior literature reports, we focus on and elucidate the simultaneous evolution of both degree of reduction and catalytic function of high-surface-area cerium oxide upon exposure to ethanol. Specifically, we use four distinct sets of transient kinetic experiments, the quantitative analysis of which

captures, with clarity, a progressive increase in propensity towards catalytic nonoxidative dehydrogenation with degree of reduction. To this end, we describe in Section 3.1 the implications of switching from aerobic to anaerobic conditions; in Section 3.2, we analyze the induction period for anaerobic dehydrogenation; the effect of prereduction under hydrogen at progressively greater temperatures on anaerobic transients is presented in Section 3.3, the latter half of which discusses the use of alpha hydrogen-free oxygenates that appear to selectively titrate dehydrogenative routes to acetaldehyde formation. All four sets of transient experiments reported herein point to the near-exclusive prevalence of oxidative routes over oxidized ceria surfaces, and an evolution toward dehydrogenative routes upon progressive surface reduction.

2. Experimental

2.1. Catalyst synthesis

Bulk cerium oxide was prepared using the procedure reported by Schimming et al. [6]. Precipitation of cerium oxide was carried out by adding cerium (III) nitrate hexahydrate (Acros Organics, 99.5%) to an aqueous solution of ammonium hydroxide (ACS reagent grade, 28-30%). Specifically, a 0.1 M solution was prepared by dissolving 21.77 g of Ce(NO₃)₃·6H₂O in 498.6 g of deionized water. This solution was then added dropwise to 512 mL aqueous NH₄OH with continuous stirring at a rate of 500 rpm over the course of 1.2 ks. The precipitate was filtered using a hand vacuum pump and rinsed twice with 50 mL deionized water per 200 mL of solution filtered. The obtained powder was dried overnight at 373 K in an oven and calcined in a muffle furnace for 14.4 ks at 773 K under 3.33 cm³ s⁻¹ air (Matheson, zero-grade) with a ramp rate of 0.083 K s^{-1} —a procedure similar to those in other reports in the literature [6,41]. A mass of 8.4 g of catalyst was recovered in the process and used for characterization and reactivity studies.

2.2. Material characterization

Powder X-ray diffraction patterns were collected on a Rigaku SmartLab Diffractometer using CuK α radiation (40 kV, 30 mA) in the range of 2θ = 20° – 80° with a step size of 0.02° and a scan rate of 0.167°s⁻¹. N₂ physisorption isotherms were measured using a Micromeritics 3 Flex instrument at 77 K, with the samples degassed at 473 K and 10.67–13.33 Pa for 14.4 ks.

2.3. Reactivity studies

The catalyst sample (~25 mg) was loaded into a quartz tube (inner diameter 0.004 m) mounted in an insulated single-zone furnace (1060 W/115 V, Applied Test Systems Series 3210) with a thermocouple (Omega, Model KMQXL-062U-15) placed at the top of the catalyst bed connected to an Applied Test Systems temperature controller (Model 17-16907) used to control bed temperature and ramp rates. The sample was heated to 773 K at a ramp rate of 0.046 K $\rm s^{-1}$ and then pretreated under air (5 kPa $\rm O_2$) in a He flow of $0.35~\text{cm}^3~\text{s}^{-1}$ for 3.6~ks. A prereduction step, when required, was carried out after the pretreatment step, at the desired temperature under 7 kPa H2 (Matheson, UHP), 20 kPa Argon (Matheson, UHP grade, internal standard), balance He. Water formation during the prereduction step was measured using an MKS Cirrus 3.0 mass spectrometer. The sample was then cooled to reaction temperature (498 K) at 0.021 K s⁻¹ under air, for reaction over oxidized ceria, or H2 in He, for reaction over reduced ceria. Vapor-phase anaerobic dehydrogenation was carried out by feeding a mixture containing ethanol, ethane (internal standard;

2.01% in N₂, Praxair, certified standard), and He. To conduct partial oxidation of ethanol, air (1.2 kPa O₂) was added to the reaction stream. During phenol co-feed experiments, a mixture of ethanol and phenol was used. Ethanol (Sigma, 99%, ReagentPlus) or a mixture of ethanol and phenol (Sigma, 89%, ReagentPlus) was fed using a syringe pump (KD Scientific, Model 100), with tubing downstream of the syringe pump heated to 373-393 K to prevent condensation of ethanol and reaction products. Spent catalysts were regenerated at 773 K in air (5 kPa O2) in a He stream with a total flow rate of $0.35~\text{cm}^3~\text{s}^{-1}$ for 28.8 ks. Organic product molar flow rates were quantified using a flame ionization detector on an Agilent 7890B gas chromatograph equipped with a methyl-siloxane capillary column (HP-1, 30 m \times 320 μ m \times 3 μ m). Inorganic products were quantified using a thermal conductivity detector on the same GC connected to a bonded polystyrene-divinylbenzene (DVB) capillary column (HP-PLOT/Q, 30 m \times 320 μ m \times 3 μ m). Ethanol conversion was calculated by comparing total molar flow rates of carbon-containing products quantified using the GC with the inlet flow rate of ethanol.

3. Results and discussion

3.1. Aerobic-anaerobic transients

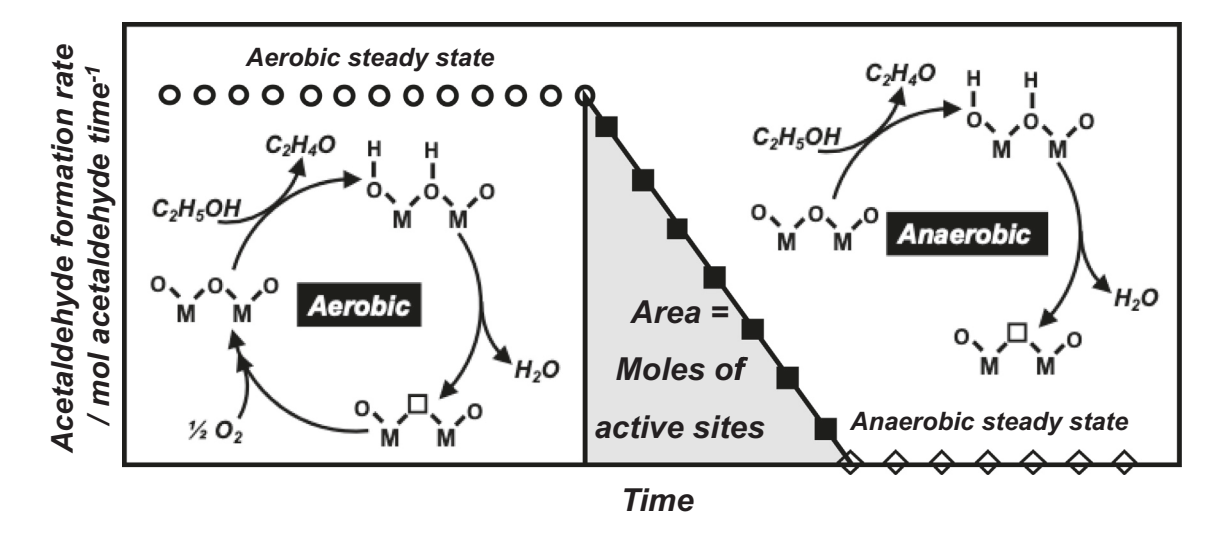
Aerobic ethanol dehydrogenation over bulk high-surface-area ceria at 498 K (0.43 kPa C_2H_5OH , 1.2 kPa O_2) leads to steady state acetaldehyde formation rates more than 50-fold greater than diethyl ether formation rates, in contrast with supported VO_x/Al_2O_3 catalysts that exhibit only a fivefold difference in acetaldehyde and diethyl ether formation rates (4 kPa C_2H_5OH , 9 kPa O_2 , 473 K) [18]. This observation is consistent with DFT studies on (111) and (100) ceria surfaces that predict acetaldehyde as the major product up to 573 K [42], and experimental studies suggesting the predominance of acetaldehyde over ethylene and diethyl ether as products at temperatures below 640 K [43]. Acetaldehyde and CO_2 are the major products observed at steady state (Fig. S6, Supporting Information), consistent with prior literature reporting acetaldehyde and CO_2 as major products during steady state aerobic ethanol experiments between 423 and 623 K [5,34].

Aerobic-anaerobic switches can be used to count sites involved in Mars-van Krevelen (MvK) redox cycles, as shown by the Baertsch and Iglesia groups for supported Ru_2O and Group V-VI

metal oxides [26,27,29]. These cycles involve vacancy creation that is preceded by hydrogen abstraction steps in the reduction half of the cycle, followed by reoxidation steps that constitute the oxidation half of the cycle (Scheme 1). Eliminating gas-phase oxygen as part of an aerobic-anaerobic switch results in a gradual decrease in acetaldehyde formation rates due to depletion of gas-phase oxygen, the dissociative adsorption of which constitutes the oxidation half of the cycle. The absence of gas-phase oxygen results in stoichiometric aldehyde formation, the rates of which progressively decrease to zero due to the lack of non-MvK contributions to aldehyde formation (Scheme 1). Assuming one aldehyde and water molecule each are formed per reduction half cycle, the moles of active sites effecting oxidative dehydrogenation under aerobic conditions can be estimated as the cumulative moles of acetaldehyde or water formed during this transient. An accurate quantification of active sites using this method is predicated on the assumption that while the reduction half of the cycle involving surface oxygen continues to proceed, sites created upon reduction do not contribute to alkanal formation. We note that in the event that MvK cycles do not constitute the sole route to alkanal formation, a nonzero rate of alkanal formation may be measured upon switching to anaerobic conditions.

Aerobic-anaerobic ethanol switches over high-surface-area cerium oxide, unlike analogous experiments [26,27,29] for alkanol conversion over supported metal oxides result not in transient acetaldehyde formation rates that drop to negligible values, but that instead transition to a steady state value approximately half the aerobic steady state rate $(3.3 \times 10^{-4} - 1.6 \times 10^{-4} \text{ mol CH}_3\text{CHO})$ $(\text{mol Ce}_s)^{-1}$ s⁻¹, Fig. 1). Acetaldehyde formation rates can be recovered upon reintroduction of oxygen, suggesting that residual rates measured under anaerobic conditions are likely not a result of irreversible changes in catalyst structure. The reversibility of the transient behavior suggests, instead, one of two possibilities, both of which complicate the direct use of transient acetaldehyde formation rates in assessing site densities: (1) a contribution to acetaldehyde formation, in the presence of gas-phase oxygen, from non-MyK routes that cannot be eliminated merely through the removal of molecular oxygen from the feed stream, or (2) the formation of acetaldehyde via non-MvK routes that are enabled by the transient stoichiometric formation of acetaldehyde and the corresponding concurrent surface reduction.

To assess the plausibility of the former, we define and assess normalized water molar flow rates (denoted by η) based on reac-



Scheme 1. Conceptual depiction of the use of aerobic–anaerobic transients in estimating the number of active sites involved in Mars–van Krevelen cycles. Steps constituting MvK cycles operative under aerobic conditions are shown on the left, steps involved in stoichiometric oxidation occurring under anaerobic conditions are shown on the right, and the integration of acetaldehyde formation rates during the transient as a function of time yielding total site densities is depicted in the center.

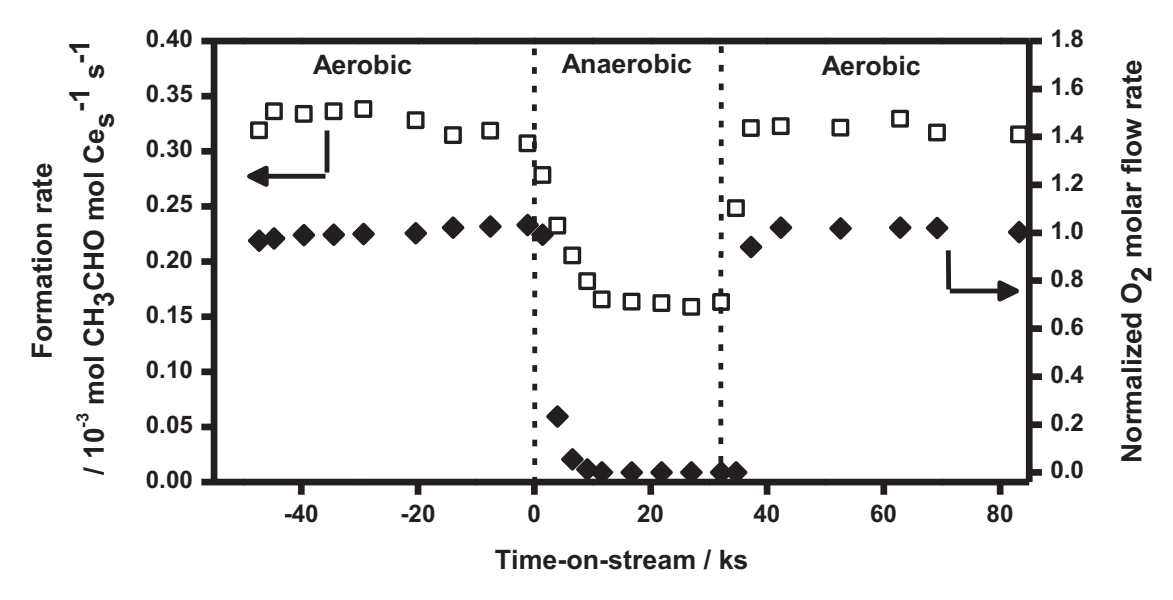


Fig. 1. Acetaldehyde formation rates and normalized oxygen molar flow rates during aerobic-anaerobic switching experiments over high-surface-area CeO₂. Hollow squares represent acetaldehyde formation rates and filled diamonds represent normalized oxygen molar flow rates. Reaction conditions: 0.43 kPa C₂H₅OH, 1.2 kPa O₂, He balance, 1.9×10^{-6} mol C₂H₅OH g_{cat}^{-1} s⁻¹, 498 K.

$$C_{2}H_{5}OH \xrightarrow{\frac{1}{2}O_{2}} C_{2}H_{4}O \xrightarrow{\frac{5}{2}O_{2}} 2CO_{2} + 3H_{2}O \qquad \eta_{0xidation} = \frac{moles\ H_{2}O}{moles\ C_{2}H_{4}O + 1.5\ moles\ CO_{2}} = 1$$

$$C_2H_5OH \longrightarrow C_2H_4O + H_2$$
 $\eta_{dehydrogenation} = \frac{moles\ H_2O}{moles\ C_2H_4O + 1.5\ moles\ CO_2} = 0$

Scheme 2. Reaction stoichiometry for partial and total ethanol oxidation (top) and ethanol dehydrogenation (bottom), and corresponding normalized water molar flow rates (η) .

tion stoichiometry. Acetaldehyde and CO₂ are the major products observed in all the transient data reported here, with one mole of water per mole of acetaldehyde formed upon partial oxidation, and 1.5 moles of water per mole of CO₂ formed upon total oxidation (Scheme 2). Ethanol dehydrogenation, on the other hand, produces acetaldehyde and hydrogen, without water as a byproduct. We define η as the molar flow rate of water divided by the sum of the molar flow rate of acetaldehyde and 1.5 times the molar flow rate of CO₂. Normalizing water molar flow rates in this manner allows us to gauge contributions from oxidative and (nonoxidative) dehydrogenative routes to acetaldehyde formation at any point during the ethanol transients. η values of 1 indicate contributions exclusively from oxidative dehydrogenation (either catalytic or stoichiometric), whereas η values of 0 indicate the exclusive occurrence of ethanol dehydrogenation. Values between 0 and 1 represent contributions from both routes, with lower values representing greater contributions from ethanol dehydrogenation compared to ethanol oxidation. We emphasize the fact that the η values reported here derived purely from reaction stoichiometry can only be used to differentiate between contributions from oxidative and nonoxidative routes: we do not use these normalized water molar flow rates in determining relative rates of oxidation and dehydrogenation- rates that remain inaccessible in the transient experiments reported in our study.

 η values near unity under steady state aerobic conditions (Fig. 2) suggest the occurrence, exclusively, of catalytic oxidation

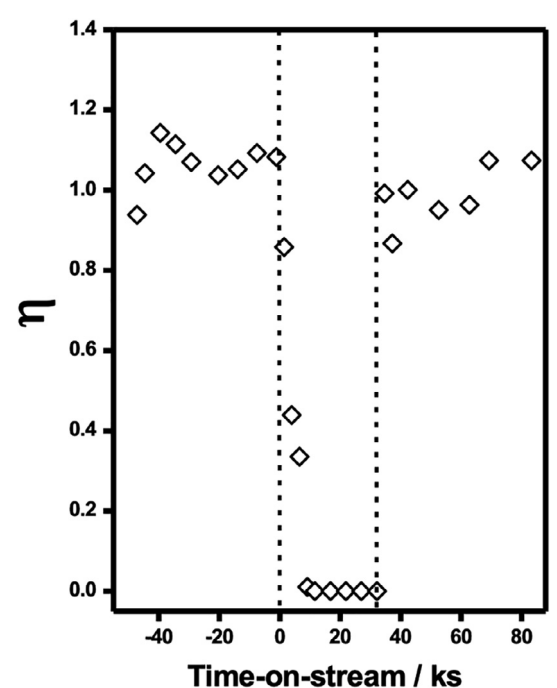


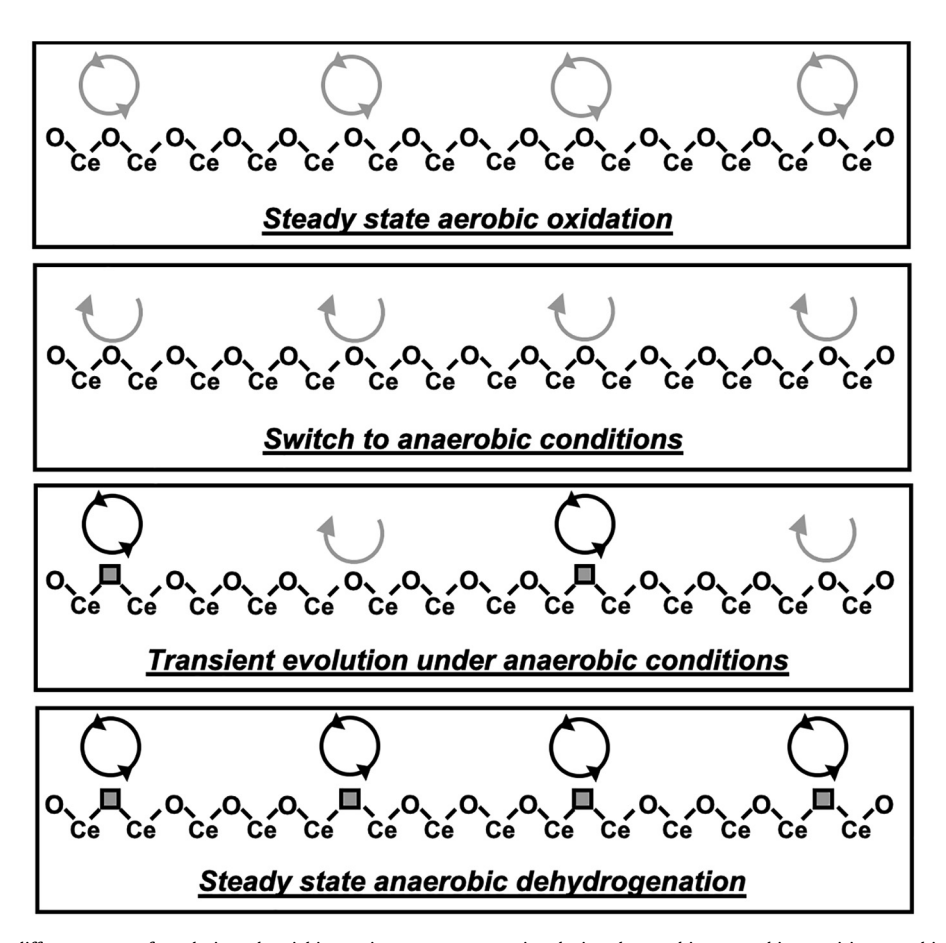
Fig. 2. Normalized water flow rate, η , measured over high-surface-area CeO₂ during aerobic-anaerobic switching experiments. Reaction conditions: 0.43 kPa C₂H₅OH, 1.2 kPa O₂, He balance, 1.9×10^{-6} mol C₂H₅OH g_{clat}^{-1} s⁻¹, 498 K.

of ethanol, and are consistent with the absence of nonoxidative routes to acetaldehyde formation in the presence of gas-phase ethanol and oxygen. Normalized water molar flow rates drop monotonically with increasing time on stream upon switching to anaerobic conditions, suggesting increasing relative contributions to acetaldehyde formation from ethanol dehydrogenation. The lack of water (or any oxygen-containing product except acetaldehyde) measured under steady state anaerobic conditions is merely reflective of the depletion of surface oxygen that could potentially participate in MvK-type redox cycles. This depletion is challenging to accurately quantify given the prevalence of finite gas-phase oxygen partial pressures during the transient (Fig. 1)—an artifact that can be overcome in the anaerobic experiments described in the next section. The transition from exclusively ethanol oxidation $(\eta \sim 1)$ before the switch to ethanol dehydrogenation $(\eta = 0)$ after the switch suggests that sites for ethanol dehydrogenation, rather than being present under aerobic conditions, are in fact created subsequent to the elimination of oxygen from the feed. It appears, therefore, that the ceria material evolves under anaerobic conditions in a manner that endows it with the ability to effectuate catalytic dehydrogenation-an ability that the native oxide is deprived of. Such an evolution toward catalytic dehydrogenation entails contributions from both catalytic and stoichiometric events to acetaldehyde formation, and preclude its transient rate of formation from being used to count active sites, as done in previous reports focusing on systems where reduction, rather than leading to a propensity to catalytic dehydrogenation, results in the elimination of acetaldehyde formation [27,29]. Correcting for this overestimation of site densities resulting from catalytic dehydrogenation requires distinguishing between catalytic and stoichiometric contributions to alkanal formation, the deconvolution of which is prevented by the nonzero oxygen partial pressures prevalent immediately after the switch to anaerobic conditions (Fig. 1).

Based on aerobic oxidation η values that decrease from unity to zero upon switching to anaerobic conditions, and the nonzero acetaldehyde formation rates under the latter conditions, we hypothesize that the aerobic–anaerobic transition shown in Fig. 1 is a result of an evolution in surface catalytic function from oxidation (in the presence of gas-phase oxygen) to dehydrogenation over a reduced surface created as a result of stoichiometric acetaldehyde formation (Scheme 3). In the next section, we analyze quantitatively, from the standpoint of both the degree of surface reduction and the relative contributions of oxidative and nonoxidative routes, the induction period observed under anaerobic conditions. These analyses allow an elimination of complications in data interpretation arising from the presence of gas-phase oxygen subsequent to aerobic–anaerobic switches.

3.2. Anaerobic dehydrogenation of ethanol

Anaerobic dehydrogenation of ethanol, subsequent to an induction period, resulted in steady state acetaldehyde rates higher than those measured in the absence of a catalyst, but comparable to those measured upon switching from aerobic to anaerobic conditions (Fig. 3a), consistent with the occurrence of catalytic nonoxidative ethanol dehydrogenation over high-surface-area ceria at 498 K. We now analyze the induction period preceding this steady



Scheme 3. Depiction of the different types of catalytic and stoichiometric processes occurring during the aerobic–anaerobic transition over high-surface-area ceria (Fig. 1). Complete circles represent catalytic cycles and incomplete curved arrows represent stoichiometric events. Gray circles/semicircles represent oxidative routes, whereas black circles represent catalytic dehydrogenation. Gray squares with black borders denote oxygen vacancies created upon stoichiometric oxidative acetaldehyde formation.

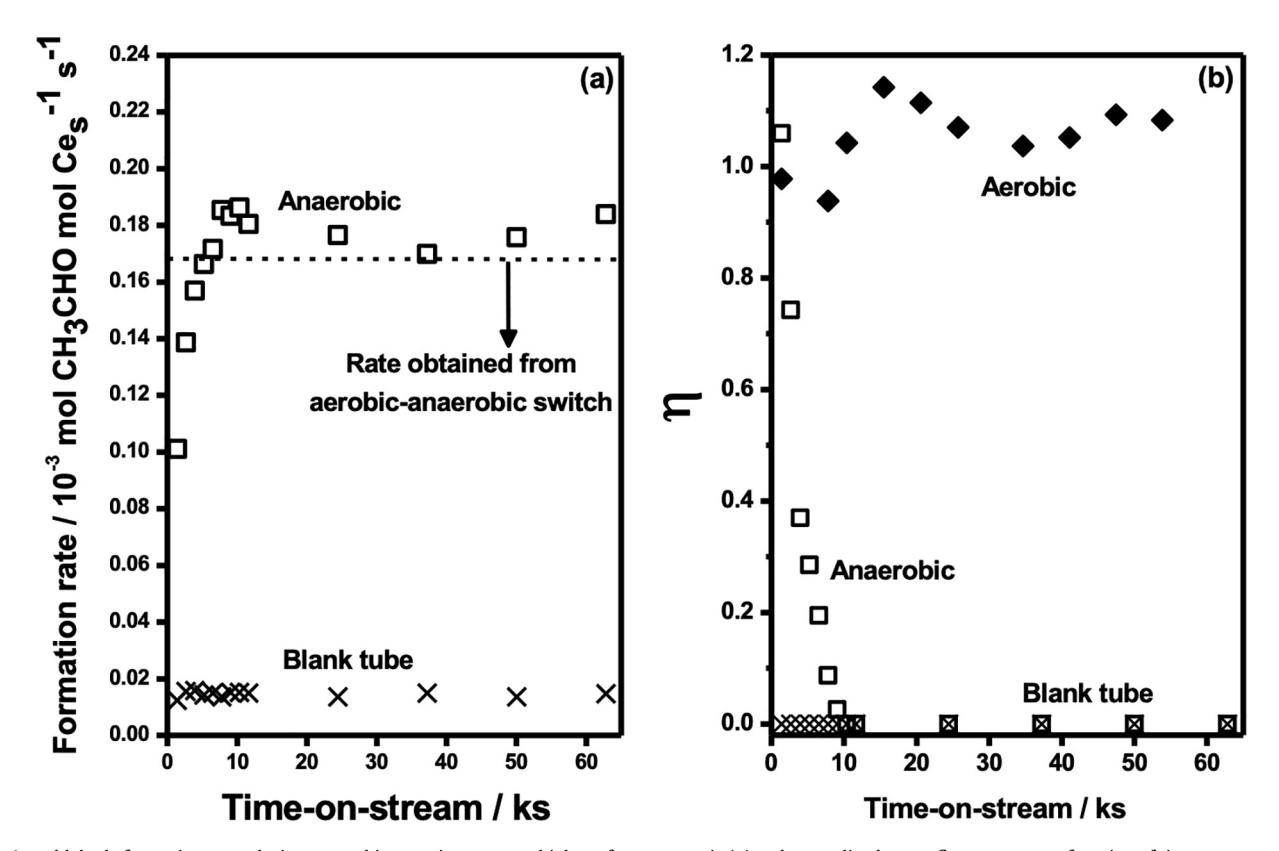


Fig. 3. Acetaldehyde formation rates during anaerobic experiments over high-surface-area ceria (a) and normalized water flow rate η as a function of time on stream during aerobic and anaerobic runs (b). The dashed line in (a) represents the anaerobic rate measured when switching from aerobic to anaerobic conditions as discussed in Section 3.1; hollow squares represent anaerobic runs, filled diamonds represent aerobic runs, and crosses represent anaerobic runs without catalyst. Reaction conditions: 0.43 kPa C_2H_5OH , O/1.2 kPa O_2 , He balance, 1.9×10^{-6} mol C_2H_5OH grant $C_$

state rate quantitatively with the goal of deciphering the nature of active sites effecting nonoxidative dehydrogenation. Acetaldehyde, water, CO₂, and butenes are the major products produced during the induction period, with water, CO₂, and butene being absent in the product stream during steady state anaerobic dehydrogenation (Fig. S7). Initial normalized water molar flow rates (corrected for C_4 formation) approximate to unity (Fig. 3b), similar to the ratios observed in the case of steady state catalytic oxidative dehydrogenation, suggesting the initial near-exclusive occurrence of the reduction half of the oxidative cycle. The decrease in η as a function of time on stream points to an evolution away from ethanol oxidation, as a consequence of depletion of surface oxygens that act as hydrogen abstractors in these reduction half-cycles. The absence of water and CO₂ as products at steady state, and the progressive decrease in η toward zero, are indicative of increasing contributions from ethanol dehydrogenation over reduced surfaces, and consistent with reduced surfaces having a greater propensity to catalyze ethanol dehydrogenation to acetaldehyde and hydrogen. Attribution of the existence of an induction period to depletion in surface oxygen is further supported by the equivalence between time scales required for elimination of oxygen imbalances and those associated with reaching steady state acetaldehyde formation rates (~10 ks, Fig. 4); that is, acetaldehyde rates reach steady state values only after sufficient reduction halfcycles have occurred to render further surface oxygen removal implausible.

Although emphasizing the correlation between surface oxygen vacancy formation and catalytic acetaldehyde formation, the data in Fig. 4 leave open multiple methods for quantifying oxygen vacancy densities. These methods for the integration of oxygen imbalances as a function of time provide additional specific

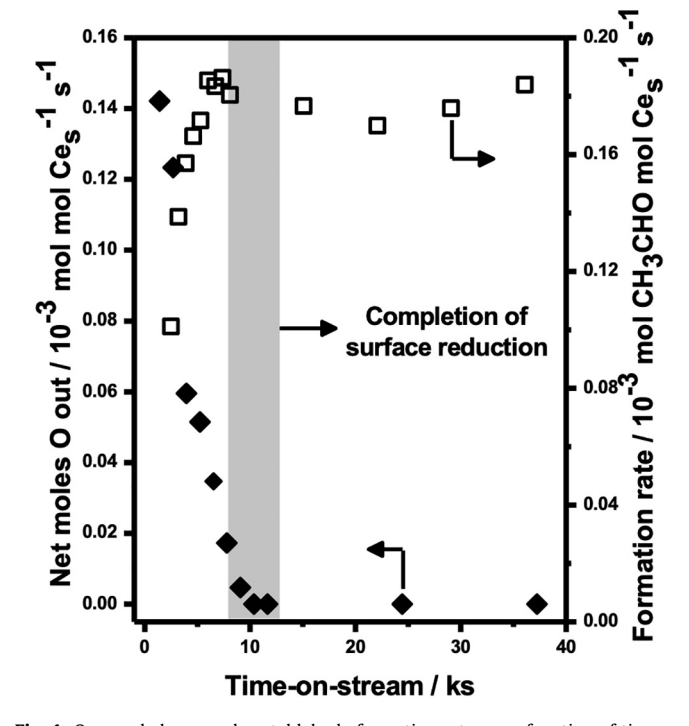


Fig. 4. Oxygen balance and acetaldehyde formation rates as a function of time on stream under anaerobic conditions. Filled diamonds represent net moles of oxygen per unit time and hollow squares represent acetaldehyde formation rates. Reaction conditions: 0.4 kPa C_2H_5OH , He balance, 1.9×10^{-6} mol C_2H_5OH g⁻¹_{cat} s⁻¹, 498 K.

insights into the relation between surface reduction and ethanol dehydrogenation. Two distinct methods for calculating vacancy

$$C_2H_5OH + O_s \rightarrow C_2H_4O + H_2O$$

 $C_2H_5OH + 6O_s \rightarrow 2CO_2 + 3H_2O$

Moles of O-vacancies created = cumulative moles of acetaldehyde formed $+ 3 \times \text{cumulative}$

moles of CO₂ formed (1)

Moles of O-vacancies created = cumulative moles of H_2O formed + 1.5 \times cumulative moles of

CO₂ formed (2)

Scheme 4. Reaction stoichiometry for ethanol partial oxidation (top) and total oxidation (bottom) with the involvement of surface oxygens (O_s).

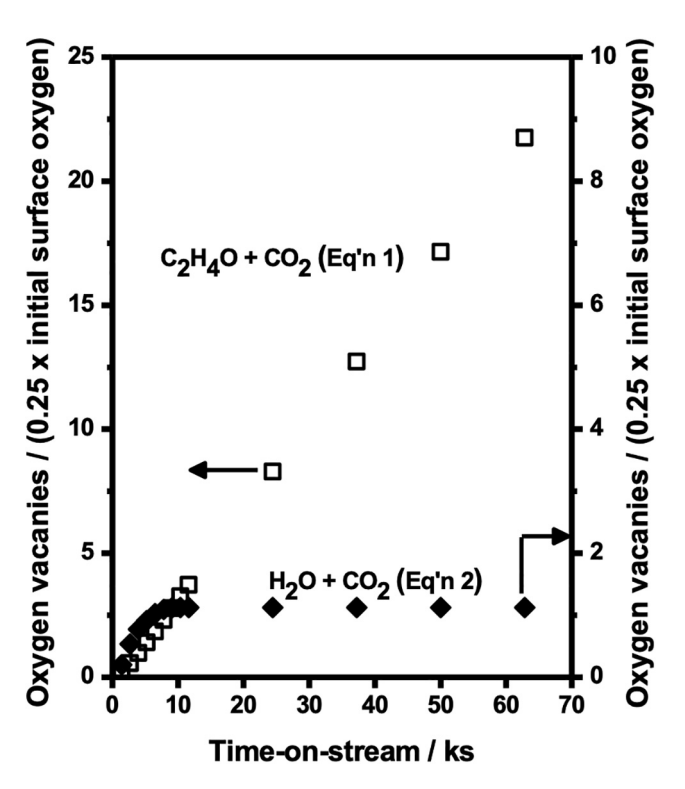
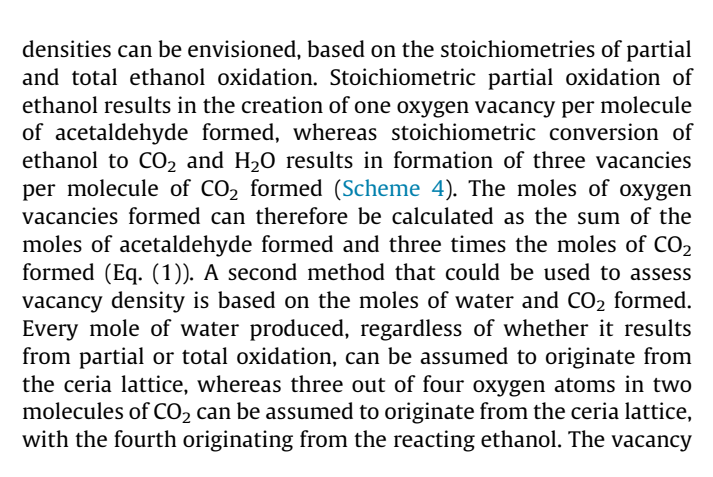


Fig. 5. Normalized vacancy densities during anaerobic transients over high-surface-area ceria. Hollow squares represent values calculated using Eq. (1) and filled diamonds represent values calculated using Eq. (2). Reaction conditions: 0.4 kPa C_2H_5OH , He balance 1.9×10^{-6} mol C_2H_5OH g_{cat}^{-1} s^{-1} , 498 K.



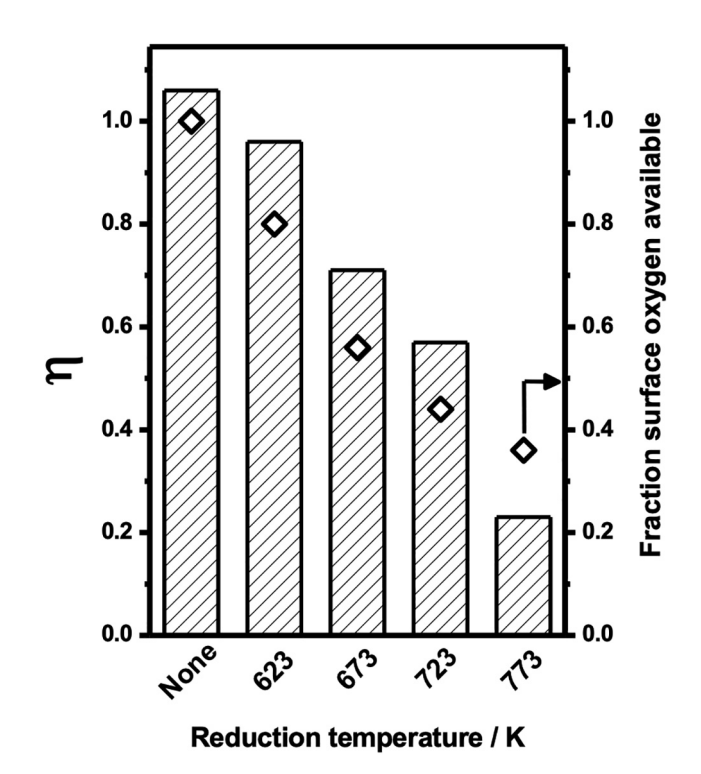


Fig. 6. Normalized initial water molar flow rates and fraction of surface oxygen available after H_2 pretreatments as a function of prereduction temperature. Prereduction conditions: 7 kPa H_2 , 20 kPa Ar, 623–773 K. Reaction conditions: 0.43 kPa C_2H_5OH , balance He, 1.9×10^{-6} mol C_2H_5OH g_{cat}^{-1} s $^{-1}$, 498 K.

density can then be calculated as the sum of the moles of water formed and 1.5 times the moles of CO_2 formed (Eq. (2)). Note that in applying this equation, the oxygen atom from the ethanol molecule is assumed to desorb from the surface as CO_2 , not water. The transfer of this oxygen atom to water would require cleavage of the carbon–oxygen bond, the possibility of which has already been accounted for when correcting for the C_4 formation rate.

Fig. 5 shows normalized vacancy densities, calculated as the number of vacancies created normalized by one-fourth the number of surface oxygens available before exposure to ethanol, assuming the entire surface to be composed solely of (111) facets purported to be the most stable ones in the case of cerium oxide [44–50]. Two more assumptions are made in calculating these normalized vacancy densities: (1) one in every four surface oxygen atoms can be eliminated upon complete reduction, corresponding to

every surface cerium atom being in the + 3 oxidation state [3,51– 54], and (2) reduction is limited exclusively to the surface due to the lack of bulk oxygen mobility at 498 K [6,33,44,48,50,55-57]. Normalization by one-fourth of total surface oxygen implies that these vacancy densities assume a value of one when the surface is completely reduced. Normalized vacancy densities calculated using CO₂ and water as descriptors of surface reduction (Eq. (2)) increase with time on stream, but plateau at a value of 1 (Fig. 5), suggesting complete reduction of the ceria surface during the anaerobic induction period. Vacancy densities calculated using acetaldehyde and CO₂ as descriptors (Eq. (1)), on the other hand, increase monotonically with time, exceeding values that are plausible even upon complete surface reduction. This inconsistency between the two normalized vacancy densities can be understood in the context of catalytic and stoichiometric processes that occur during the anaerobic induction period, and are depicted in Scheme 2. Vacancy densities calculated using acetaldehyde and CO₂ molar flow rates keep increasing as a function of time beyond values corresponding to complete surface reduction because acetaldehyde, unlike water and CO₂, is produced both catalytically and stoichiometrically. Such nonstoichiometric formation of acetaldehyde in anaerobic transients renders the use of its formation rate in vacancy density calculations inaccurate, just as integrated acetaldehyde formation rates are nonrigorous descriptors of the degree of surface reduction in aerobic-anaerobic switching experiments (Sect. 3.1). The use of CO₂ and water—products exclusively of stoichiometric events—on the other hand, provide not only vacancy densities that are plausible, but also ones that correspond, subsequent to the induction period, to complete surface reduction (Fig. 5). Anaerobic experiments reported here are therefore consistent with surface reduction originating from the reduction half of the ethanol oxidation cycle creating sites that then effect ethanol dehydrogenation. Next, we assess the use of high-temperature hydrogen pretreatments and alpha and beta hydrogen-free titrants, respectively, to manipulate the density of these sites before and after exposure to ethanol.

3.3. Controlling the density of sites effecting oxidative and nonoxidative routes

Hydrogen treatments have been used in previous research to create oxygen vacancies on ceria materials, with two peaks commonly observed in temperature-programmed reduction experiments [6,10,33,55]. The low-temperature peak (typically 713-773 K) has been attributed to surface reduction and the hightemperature peak (typically 998-1023 K) to bulk reduction, an inference supported in part by correlations between the area of the low-temperature peak and ceria surface area [10], and DFT studies suggesting the need for higher temperatures to achieve bulk vacancy creation [44,48,57]. A relationship having already been established between the degree of surface reduction and the prevalence of catalytic ethanol dehydrogenation, the existence of this well-defined temperature range in which the degree of surface reduction can be controlled through the use of hydrogen treatments could potentially allow us to tune, prior to exposure to ethanol, the density of active sites effecting dehydrogenation. We use a temperature range of 623-773 K for these hydrogen treatments, with the goal of limiting reduction to the ceria surface, avoiding complications originating from bulk oxygen mobility and vacancy creation/destruction, as discussed above. Normalized vacancy densities ranging from 0.2 to 0.64 were achieved using treatment temperatures from 623 to 773 K, with increasing hydrogen pretreatment temperatures leading to higher vacancy densities (Fig. S8 and Table S2). These vacancy densities are consistent with the restriction of vacancy creation to the surface, as expected based on prior literature discussed above. The propensity of reduced sur-

faces to effect ethanol dehydrogenation, as inferred from the anaerobic and aerobic transients described above, imply that vacancies generated during these pretreatments should increase the relative initial preponderance of catalytic dehydrogenation compared to stoichiometric oxidation. Initial normalized water molar flow rates that decrease monotonically with increasing hydrogen pretreatment temperature (Fig. 6), and that track with the normalized fraction of available surface oxygen after pretreatment (assuming 25% of surface oxygen is available for C-H/O-H bond scission), are consistent with progressively greater initial contributions from dehydrogenative routes with increasing treatment temperature. We posit that this increasing propensity of prereduced surfaces to effect dehydrogenation is similar in origin to the evolution of surface catalytic function that occurs as a function of time on stream upon exposure to ethanol both in the presence and in the absence of hydrogen pretreatments. The hydrogen treatments serve merely to create part of the dehydrogenation functionality that is otherwise exclusively generated as a result of stoichiometric oxidative dehydrogenation; that is, the higher the treatment temperature, the lower the fraction of the surface that is reduced by ethanol, rather than hydrogen.

Oxygen vacancy densities after hydrogen pretreatment and anaerobic dehydrogenation were calculated by integrating measured water molar flow rates and by using Eq. (2), respectively, with the goal of verifying this assertion. Whereas vacancy densities after hydrogen treatment increased monotonically with treatment temperature, vacancy densities calculated from Eq. (2) showed the opposite trend (Fig. 7), with the latter corresponding precisely to the densities that would be required to ensure complete reduction of the surface given the varying degrees of partial reduction upon treatment under hydrogen. These trends suggest an identical degree of reduction of the ceria catalyst after both steps have occurred, with the pretreatment temperature determining merely its distribution between that effected by hydrogen and by ethanol. Pretreatment at higher temperatures leads to lower densities of available surface oxygens that participate in the reduction half of the oxidative cycle, accounted for in the vacancy density calculations utilizing Eq. (2).

All three sets of transient experiments discussed so far are consistent with a greater propensity of reduced surfaces to effect ethanol dehydrogenation— a propensity that can be accessed through the use of high-temperature hydrogen pretreatments. These hydrogen pretreatments, however, do not allow control over site

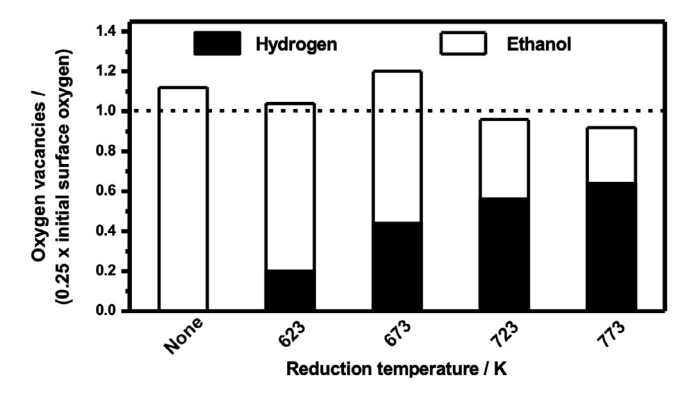


Fig. 7. Effect of prereduction temperature on normalized oxygen vacancy densities after hydrogen pretreatment and anaerobic ethanol dehydrogenation. Filled bars represent vacancies created upon reduction under hydrogen, and empty bars represent vacancies created in the presence of ethanol. Vacancy densities after hydrogen treatments were calculated by integrating water molar flow rates and those after ethanol dehydrogenation were calculated using Eq. (2). Prereduction conditions: 7 kPa $\rm H_{2}$, 20 kPa $\rm Ar$, 623–773 K; reaction conditions: 0.43 kPa $\rm C_2H_5OH$, balance He, $\rm 1.9 \times 10^{-6}$ mol $\rm C_2H_5OH$ $\rm g_{cal}^{-1}$ s⁻¹, 498 K.

Scheme 5. Hypothesized steps involved in ethanol dehydrogenation/dehydration over oxygen vacancies on ceria surfaces (top) and titration of oxygen vacancies using phenol resulting in the formation of persistent phenoxide intermediates (bottom).

β-H abstraction

densities after exposure to ethanol, the evolution of which is dependent purely on the rates of the reduction half cycle. Another approach to tuning the relative preponderance of oxidative and dehydrogenative routes is to titrate selectively, in situ, sites effecting catalytic dehydrogenation. Assuming that the occurrence of catalytic ethanol dehydrogenation is predicated on the availability of oxygen vacancies created upon surface reduction, and based on prior literature assessing the role of oxygen vacancies in alkanol adsorption/dehydrogenation [37,38,58-60], a sequence of steps such as that shown in Scheme 5 can be envisioned for ethanol dehydrogenation/dehydration. Ethanol adsorbs onto an oxygen vacancy in a step responsible for the cleavage of the oxygen-hydrogen bond, forming an ethoxide intermediate [5,38-40,58,60]. The ethoxide intermediate can undergo α-hydrogen abstraction to form acetaldehyde or β-hydrogen abstraction to form ethylene, with subsequent steps involving hydrogen or water desorption, respectively, to regenerate the oxygen vacancy to complete the catalytic cycle.

We hypothesize that the presence of oxygenates deprived of abstractable α - and β -hydrogens can lead to the formation of persistent alkoxide intermediates; the persistence of these intermediates, in contrast with ethoxide intermediates endowed with abstractable α - and β -hydrogens, can result in the poisoning of sites effecting ethanol dehydrogenation (Scheme 5, bottom), while potentially leaving unhindered the ability of the surface to effect the reduction half of the oxidative turnover. We choose for this purpose phenol, an oxygenate that has no α -hydrogens, no β -hydrogens that can be abstracted without breaking aromaticity, and one that has previously been proposed to adsorb onto oxygen vacancies on reducible metal oxide surfaces [6,61]. The presence of significant partial pressures of hydrogen in the

gas phase in these literature reports leads to the cleavage of carbon–oxygen bonds, rendering plausible the possibility of oxygen vacancies being covered with phenoxide intermediates insusceptible to C–O bond cleavage in the absence of significant pressures of gas-phase hydrogen. We discuss next the effect of co-feeding phenol during anaerobic dehydrogenation of ethanol, and assess its effect from the standpoint of relative contributions from oxidative and nonoxidative routes in the presence of α – and β –hydrogen–free titrants.

Co-feeding 0.27 kPa phenol (phenol:ethanol molar ratio 0.7) leads to acetaldehyde formation rates that decrease with time on stream (Fig. 8a), in contrast with formation rates in the absence of phenol co-feeds that increase with time on stream due to increasing contributions from nonoxidative turnovers occurring over reduced surfaces under anaerobic conditions. Decreasing acetaldehyde formation rates that plateau at values corresponding to those measured in the absence of catalyst suggest a reduction in the density of sites responsible for catalytic nonoxidative dehydrogenation, but in and of itself neither exclude nor prove the prevalence of stoichiometric oxidative routes toward acetaldehyde formation. n values in the absence of phenol co-feeds decrease with increasing degree of reduction (Figs. 6 and 8b), suggesting increasing relative contributions of nonoxidative turnovers to measured acetaldehyde formation rates upon surface reduction. In contrast, η values of unity in the presence of phenol persist through progressive surface reduction (Fig. 8b), suggesting minor (if any) contributions from nonoxidative dehydrogenation, and that acetaldehyde formation in the presence of phenol co-feeds originates predominantly from the reduction half of the oxidative cycle. Greater variability in η values close to complete reduction in Fig. 8b may merely be a consequence of increasing relative contributions from

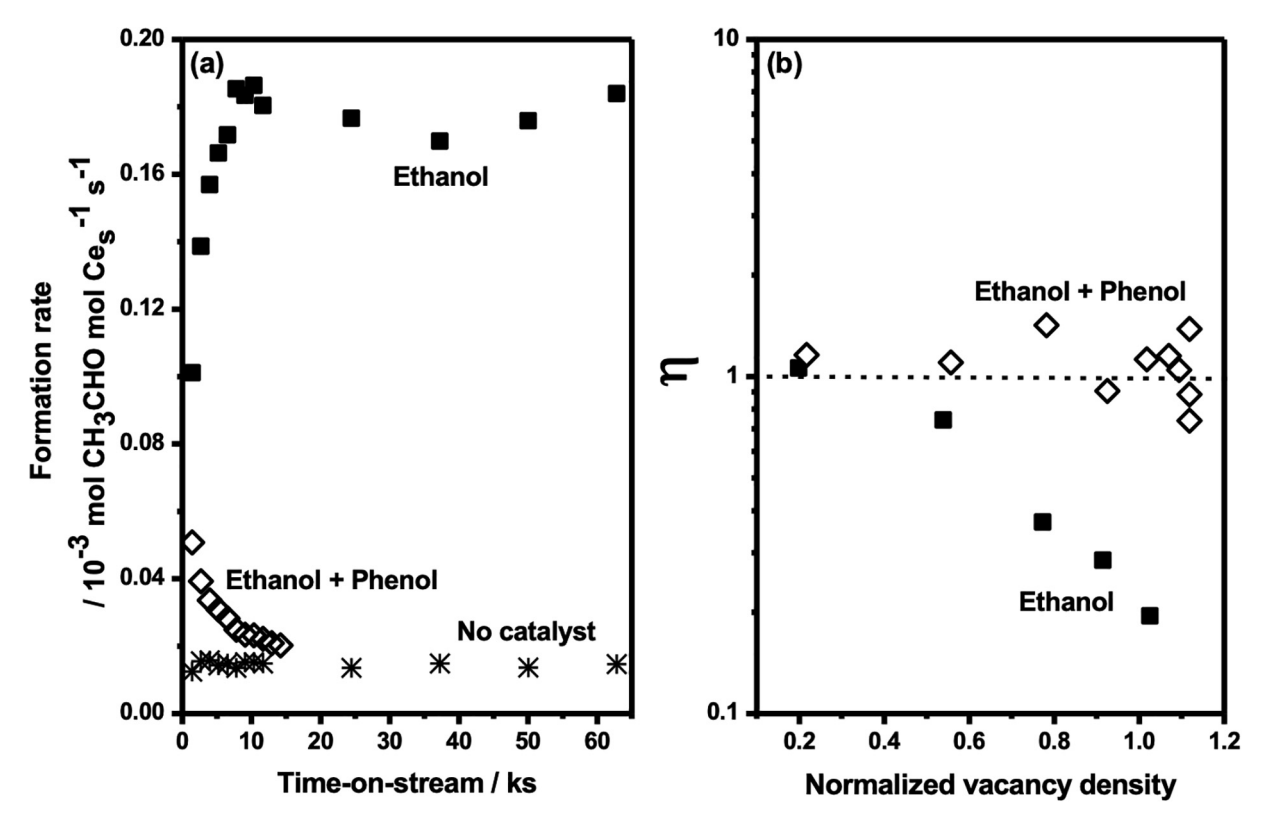


Fig. 8. Acetaldehyde formation rates (a) and normalized water flow rates (b) over high-surface-area ceria with and without phenol co-feeds, and without phenol co-feeds in the absence of catalyst. Reaction conditions: 0.43 kPa C_2H_5OH , 0.27 kPa Phenol, He balance, 1.9×10^{-6} mol C_2H_5OH g_{cat}^{-1} s⁻¹, 1.3×10^{-6} mol phenol g_{cat}^{-1} s⁻¹, 498 K.

gas phase noncatalytic dehydrogenation that render rigorous deconvolution of oxidative and nonoxidative routes highly challenging under the conditions used in this study.

η values in Fig. 8b are consistent with the selective elimination of oxygen vacancies involved in effecting ethanol dehydrogenation upon co-feeding phenol, but do not conclusively demonstrate its effect on the total number of reduction half cycles. In Section 3.1 we described two methods for assessing vacancy density, one based on acetaldehyde and CO₂ formation rates (Eq. (1)), and the other on water and CO₂ formation rates (Eq. (2)), with Eq. (2) providing plausible vacancy density values, and Eq. (1) providing implausible ones that exceed those corresponding to complete surface reduction. The reason underlying overestimation of surface reduction when Eq. (1) is used is the formation of acetaldehyde through both catalytic and stoichiometric routes, only a fraction of which can legitimately be used in the estimation of vacancy densities. If the possibility exists, however, of selectively eliminating catalytic routes to acetaldehyde formation, while still permitting the effectuation of stoichiometric routes, it can be envisioned that the use of Eq. (1) (acetaldehyde and CO₂) may also provide accurate vacancy density estimates analogous to those from Eq. (2) (CO₂ and water). Vacancy densities in the presence of phenol co-feeds calculated using Eqs. (1) and (2) show identical trends as a function of time on stream, and plateau at values corresponding to complete surface reduction (Fig. 9), consistent not only with the selective elimination of catalytic ethanol dehydrogenation but also with an imperceptible effect on the total number of stoichiometric partial and total oxidation events; unlike in the absence of phenol co-feeds, where only CO₂ and water are formed stoichiometrically, in the presence of phenol co-feeds, all three products-acetaldehyde, water, and CO2-are produced through stoichiometric, not catalytic events. Additionally, insensitivity of vacancy density profiles to the presence of phenol (Fig. 9) reem-

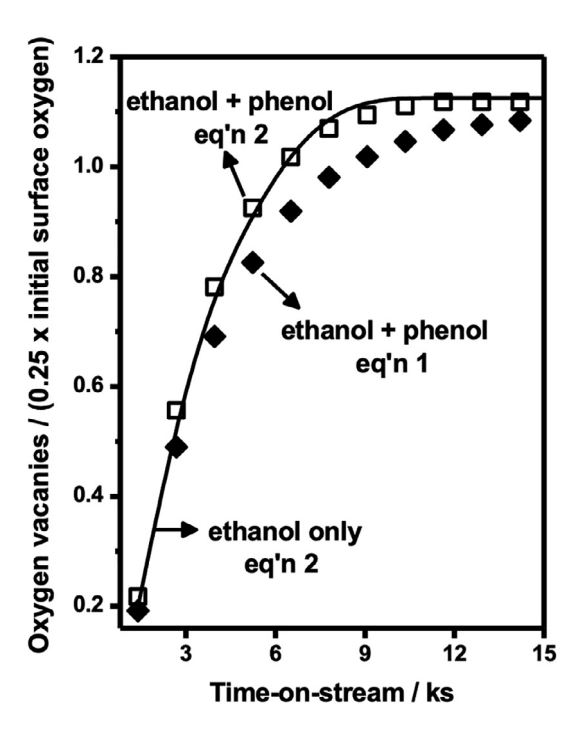


Fig. 9. Normalized vacancy densities over bulk high-surface-area ceria in the presence of phenol co-feeds calculated using Eqs. (1) (filled diamonds) and (2) (hollow squares). The solid line represents vacancy densities in the absence of phenol co-feeds, estimated using Eq. (2). Reaction conditions: 0.43 kPa C_2H_5OH , 0.27 kPa phenol, balance He, 1.9×10^{-6} mol C_2H_5OH g_{cat}^{-1} s⁻¹, 1.3×10^{-6} mol phenol g_{cat}^{-1} s⁻¹, 498 K.

phasize the negligible effect of phenol on the ability of the oxidized surface to effect partial oxidation—effects that would likely have been reflected in changes in the time scale of surface reduction.

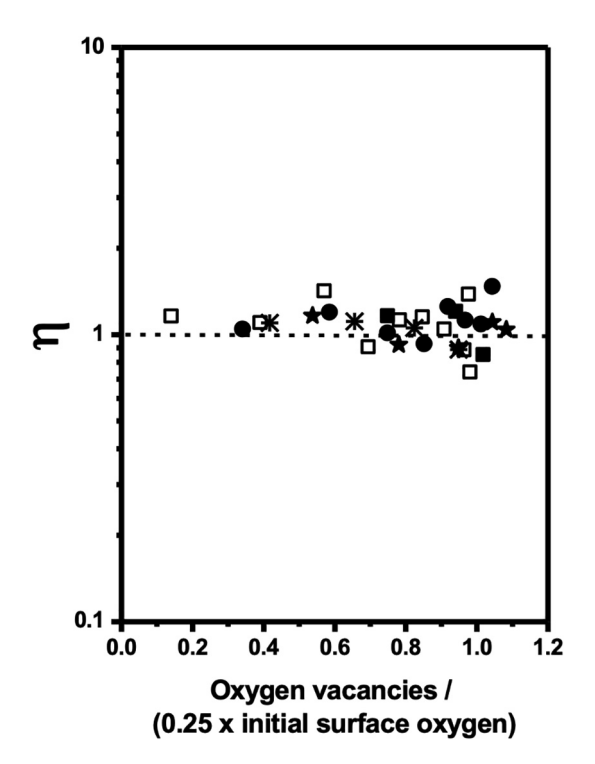


Fig. 10. Evolution of η with fractional surface reduction at various prereduction temperatures: no pretreatment (hollow squares), 623 K (filled circles), 673 K (crosses), 723 K (filled stars), 773 K (filled squares). Prereduction conditions: 7 kPa H₂, 20 kPa Ar, 623–773 K; reaction conditions: 0.4 kPa C₂H₅OH, 0.27 kPa phenol, balance He, 1.9×10^{-6} mol C₂H₅OH g_{cat}^{-1} s⁻¹, 1.3×10^{-6} mol phenol g_{cat}^{-1} s⁻¹, 498 K.

As shown above, hydrogen pretreatments can be used to control the density of sites mediating nonoxidative turnovers before exposure to ethanol, and phenol co-feeds can be used to control site densities in the presence of ethanol. Next, we probe whether a fraction of the ceria surface can be reduced under hydrogen before

exposure to ethanol, and the remaining fraction reduced under ethanol and phenol in the absence of catalytic dehydrogenation. Hydrogen pretreatment protocols similar to those described earlier in this section were used, and resulted consistently in η values in the vicinity of 1 (Fig. 10), reemphasizing the negligibility of catalytic (dehydrogenative) contributions to measured acetaldehyde formation rates in the presence of phenol, regardless of initial degree of reduction. Additionally, the fraction of the ceria surface left unreduced after high-temperature hydrogen pretreatment is entirely reduced upon exposure to ethanol and phenol, as reflected by normalized vacancy densities approximating unity after the two steps regardless of prereduction temperature (Fig. 11). These normalized vacancy density values are independent of the method used to track vacancy creation (acetaldehyde + CO₂, Eq. (1) or water + CO₂, Eq. (2)), suggesting that all three products—CO₂, water, and acetaldehyde—are produced stoichiometrically, not catalytically, irrespective of initial vacancy density. The results point to the absence of dehydrogenative turnovers even when ceria surfaces that are significantly reduced (normalized vacancy density = 0-0.62) are exposed to ethanol and phenol, despite the initial prevalence of oxygen vacancies that allow the effectuation of these dehydrogenative turnovers, in contrast with results noted in the absence of phenol (Fig. 7), where only products produced in stoichiometric events can be used in determining vacancy densities (Eq. (2)). Both methods for calculating vacancy densities yield values that correspond to the number of surface oxygens available for abstracting hydrogen, reiterating the insensitivity of both the timescales and prevalence of oxidative half cycles to the presence of phenol (Fig. 11). Increasing hydrogen pretreatment temperatures merely increase the fraction of sites titrated immediately upon exposure to ethanol-phenol mixtures, and decrease those that are titrated subsequent to acetaldehyde and/or CO2 formation. The titration of these vacancies, independent of their provenance (reduction in H₂ or ethanol), points to the potentially broad utility of α - and β -hydrogen-free titrants in the context of counting oxygen vacancies mediating catalytic turnovers over reducible metal oxides.

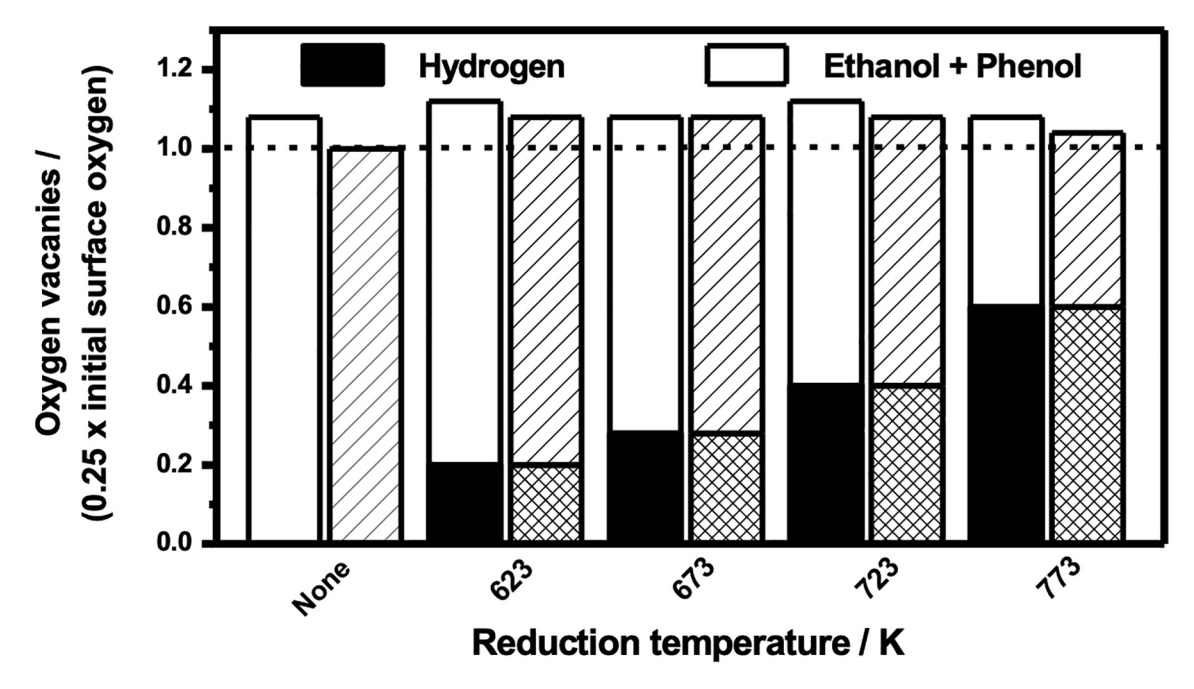


Fig. 11. Fractional surface reduction by hydrogen during the prereduction step and anaerobic ethanol dehydrogenation in the presence of phenol using Eqs. (1) (left bars) and (2) (right bars). When using eq. 1, filled bars represent reduction under hydrogen and empty bars represent reduction under ethanol and phenol. When using eq. 2, densely shaded bars represent reduction under hydrogen and sparsely shaded bars represent reduction under ethanol and phenol. Prereduction conditions: 7 kPa H₂, 20 kPa Ar, 623–773 K; reaction conditions: 0.4 kPa C_2H_5OH , 0.27 kPa phenol, He balance, 1.9×10^{-6} mol C_2H_5OH g_{cat}^{-1} s^{-1} , 1.3×10^{-6} mol phenol g_{cat}^{-1} s^{-1} , 498 K.

4. Conclusions

Upon switching from aerobic to anaerobic conditions, high surface area ceria exhibits an evolution to a steady state rate reflective of nonoxidative dehydrogenation, rather than a negligible rate, as would be expected in the absence of non-MvK contributions to acetaldehyde formation. The same steady state rate can be accessed subsequent to an induction period under anaerobic conditions, the time scale of which matches that for oxygen removal from the surface. Water and CO₂ formation rates serve as rigorous descriptors of vacancy density, unlike acetaldehyde and CO2 formation rates, which lead to implausibly high vacancy densities, pointing to the prevalence of both stoichiometric oxidative and catalytic dehydrogenative routes to acetaldehyde formation under anaerobic conditions. Normalized water molar flow rates that decrease monotonically from unity to zero evidence a greater propensity for reduced surfaces to effect dehydrogenative turnovers—a propensity that can just as effectively be accessed using high-temperature hydrogen pretreatments that create surface oxygen vacancies prior to exposure to ethanol. Active sites effecting catalytic nonoxidative ethanol dehydrogenation can be selectively titrated using phenol co-feeds, with imperceptible consequences on the prevalence and timescale of oxidative half cycles. Complete titration of oxygen vacancies can be accomplished in the presence of phenol co-feeds regardless of initial vacancy density—a fact reflected in the exclusive prevalence of oxidative routes in the presence of phenol, regardless of H₂ prereduction temperature. The combination of quantitative transient kinetic analyses used here is broadly applicable within the field of bulk oxide catalysis, and points to avenues for the water-free dehydrogenation of alkanols over reducible metal oxide surfaces.

Declaration of Competing Interest

The authors declare that they have no known competing financial interests or personal relationships that could have appeared to influence the work reported in this paper.

Acknowledgements

The authors acknowledge support from the National Science Foundation (CBET 1916133), as well as UH startup funds that were used to carry out this research. The authors declare no competing financial interest.

Appendix A. Supplementary data

Supplementary data to this article can be found online at https://doi.org/10.1016/j.jcat.2020.08.023.

References

- [1] K. Reinhardt, H. Winkler, Cerium mischmetal, cerium alloys, and cerium compounds, Ullmann's Encyclopedia of Industrial Chemistry 8 (2012) 531–621, https://doi.org/10.1002/14356007.a06.
- [2] J. Beckers, G. Rothenberg, Sustainable selective oxidations using ceria-based materials, Green Chem. 12 (2010) 939–948, https://doi.org/10.1039/c000191k.
- [3] L. Vivier, D. Duprez, Ceria-based solid catalysts for organic chemistry, ChemSusChem 3 (2010) 654–678, https://doi.org/10.1002/cssc.201000054.
- [4] A. Trovarelli, Catalytic Properties of Ceria, Catal. Rev. 38 (2006) 439–520, https://doi.org/10.1080/01614949608006464.
- [5] M. Li, Z. Wu, S.H. Overbury, Surface structure dependence of selective oxidation of ethanol on faceted CeO₂ nanocrystals, J. Catal. 306 (2013) 164– 176, https://doi.org/10.1016/j.jcat.2013.06.019.
- [6] S.M. Schimming, O.D. Lamont, M. König, A.K. Rogers, A.D. D'Amico, M.M. Yung, C. Sievers, Hydrodeoxygenation of guaiacol over ceria-zirconia catalysts, ChemSusChem 8 (2015) 2073–2083, https://doi.org/10.1002/cssc.201500317.
- [7] N. Yi, R. Si, H. Saltsburg, M. Flytzani-Stephanopoulos, Steam reforming of methanol over ceria and gold-ceria nanoshapes, Appl. Catal. B Environ. 95 (2010) 87–92, https://doi.org/10.1016/j.apcatb.2009.12.012.

- [8] E. Aneggi, M. Boaro, C. De Leitenburg, G. Dolcetti, A. Trovarelli, Insights into the redox properties of ceria-based oxides and their implications in catalysis, J. Alloys Compd. 408–412 (2006) 1096–1102, https://doi.org/10.1016/ i.iallcom.2004.12.113
- [9] M. Shelef, G.W. Graham, R.W. McCabe, Ceria and other oxygen storage components in automotive catalysts, Catal. Sci. Ser. 2 (2002) 343–375, https:// doi.org/10.1142/9781860949654 0010.
- [10] H.C. Yao, Y.F.Y. Yao, Ceria in automotive exhaust catalysts. I. Oxygen storage, J. Catal. 86 (1984) 254–265, https://doi.org/10.1016/0021-9517(84)90371-3.
- [11] M. O'Connell, M.A. Morris, New ceria-based catalysts for pollution abatement, Catal. Today 59 (2000) 387–393, https://doi.org/10.1016/S0920-5861(00) 00303-5.
- [12] G. Kim, Ceria-Promoted Three-Way Catalysts for Auto Exhaust Emission Control, Ind. Eng. Chem. Prod. Res. Dev. 21 (1982) 267–274, https://doi.org/ 10.1021/i300006a014.
- [13] C.D. Baertsch, K.T. Komala, Y.H. Chua, E. Iglesia, Genesis of Brønsted acid sites during dehydration of 2-butanol on tungsten oxide catalysts, J. Catal. 205 (2002) 44–57, https://doi.org/10.1006/jcat.2001.3426.
- [14] P. Kostestkyy, J. Yu, R.J. Gorte, G. Mpourmpakis, Structure-activity relationships on metal-oxides: Alcohol dehydration, Catal. Sci. Technol. 4 (2014) 3861–3869, https://doi.org/10.1039/c4cy00632a.
- [15] J.F. DeWilde, C.J. Czopinski, A. Bhan, Ethanol dehydration and dehydrogenation on γ-Al₂O₃: Mechanism of acetaldehyde formation, ACS Catal. 4 (2014) 4425– 4433, https://doi.org/10.1021/cs501239x.
- [16] J.F. DeWilde, H. Chiang, D.A. Hickman, C.R. Ho, A. Bhan, Kinetics and mechanism of ethanol dehydration on γ-Al₂O₃: The critical role of dimer inhibition, ACS Catal. 3 (2013) 798–807, https://doi.org/10.1021/ cs400051k
- [17] Z. Li, B. Šmíd, Y.K. Kim, V. Matolín, B.D. Kay, R. Rousseau, Z. Dohnálek, Alcohol dehydration on monooxo W=O and Dioxo O=W=O Species, J. Phys. Chem. Lett. 3 (2012) 2168–2172, https://doi.org/10.1021/jz300885v.
- [18] B. Kilos, A.T. Bell, E. Iglesia, Mechanism and site requirements for ethanol oxidation on vanadium oxide domains, J. Phys. Chem. C 113 (2009) 2830– 2836, https://doi.org/10.1021/jp8078056.
- [19] H. Idriss, E.G. Seebauer, Reactions of ethanol over metal oxides, J. Mol. Catal. A Chem. 152 (2000) 201–212, https://doi.org/10.1016/S1381-1169(99) 00297-6.
- [20] S. Golay, R. Doepper, A. Renken, In-situ characterisation of the surface intermediates for the ethanol dehydration reaction over γ-alumina under dynamic conditions, Appl. Catal. A Gen. 172 (1998) 97–106, https://doi.org/ 10.1016/S0926-860X(98)00109-4.
- [21] M. Xu, E. Iglesia, C.R. Apestegu, D.I. Cosimo, E.T. Al, Structure and surface and catalytic properties of Mg–Al basic oxides, J. Catal. 178 (1998) 499–510.
- [22] M.P. Rosynek, R.J. Koprowski, G.N. Dellisante, The nature of catalytic sites on lanthanum and neodymium oxides for dehydration/dehydrogenation of ethanol, J. Catal. 122 (1990) 80–94, https://doi.org/10.1016/0021-9517(90) 90263-1.
- [23] C. Lahousse, F. Maugé, J. Bachelier, J.C. Lavalley, Acidic and basic properties of titania-alumina mixed oxides; Active sites for propan-2-ol dehydration, J. Chem. Soc. Faraday Trans. 91 (1995) 2907–2912, https://doi.org/10.1039/ FT9959102907.
- [24] M.A. Christiansen, G. Mpourmpakis, D.G. Vlachos, Density functional theory-computed mechanisms of ethylene and diethyl ether formation from ethanol on γ -Al₂O₃(100), ACS Catal. 3 (2013) 1965–1975, https://doi.org/10.1021/cs4002833.
- [25] G.S. Foo, Z.D. Hood, Z. Wu, Shape Effect Undermined by Surface Reconstruction: Ethanol Dehydrogenation over Shape-Controlled SrTiO₃ Nanocrystals, ACS Catal. 8 (2018) 555–565, https://doi.org/10.1021/acscatal.7b03341.
- [26] H. Nair, J.E. Gatt, J.T. Miller, C.D. Baertsch, Mechanistic insights into the formation of acetaldehyde and diethyl ether from ethanol over supported VO_x. MoO_x, and WO_x catalysts, J. Catal. 279 (2011) 144–154, https://doi.org/ 10.1016/j.icat.2011.01.011.
- [27] H. Liu, E. Iglesia, Selective oxidation of methanol and ethanol on supported ruthenium oxide clusters at low temperatures, J. Phys. Chem. B 109 (2005) 2155–2163, https://doi.org/10.1021/jp0401980.
- [28] P. Deshlahra, E. Iglesia, Methanol Oxidative Dehydrogenation on Oxide Catalysts: Molecular and Dissociative Routes and Hydrogen Addition Energies as Descriptors of Reactivity, J. Phys. Chem. C 118 (2014) 26115– 26129, https://doi.org/10.1021/jp507922u.
- [29] H. Nair, C.D. Baertsch, Method for quantifying redox site densities in metal oxide catalysts: Application to the comparison of turnover frequencies for ethanol oxidative dehydrogenation over alumina-supported VO_x, MoO_x, and WO_x catalysts, J. Catal. 258 (2008) 1–4, https://doi.org/10.1016/j.jcat.2008.05.023.
- [30] A. Beste, S.H. Overbury, Dehydrogenation of methanol to formaldehyde catalyzed by pristine and defective ceria surfaces, Phys. Chem. Chem. Phys. 18 (2016) 9990–9998, https://doi.org/10.1039/c6cp00151c.
- [31] T. Otroshchenko, S. Sokolov, M. Stoyanova, V.A. Kondratenko, U. Rodemerck, D. Linke, E.V. Kondratenko, ZrO₂-Based Alternatives to Conventional Propane Dehydrogenation Catalysts: Active Sites, Design, and Performance, Angew. Chem. Int. Ed. 54 (2015) 15880–15883, https://doi.org/10.1002/anie.201508731
- [32] E.V. Kondratenko, ZrO₂-based unconventional catalysts for non-oxidative propane dehydrogenation: Factors determining catalytic activity, J. Catal. 348 (2017) 282–290, https://doi.org/10.1016/j.jcat.2017.02.016.

- [33] F. Giordano, A. Trovarelli, C. De Leitenburg, M. Giona, A model for the temperature-programmed reduction of low and high surface area ceria, J. Catal. 193 (2000) 273–282, https://doi.org/10.1006/jcat.2000.2900.
- [34] A. Yee, S.J. Morrison, H. Idriss, A study of the reactions of ethanol on CeO₂ and Pd/CeO₂ by steady state reactions, temperature programmed desorption, and in situ FT-IR, J. Catal. 186 (1999) 279–295, https://doi.org/10.1006/ jcat.1999.2563.
- [35] C. Binet, M. Daturi, J.C. Lavalley, IR study of polycrystalline ceria properties in oxidised and reduced states, Catal. Today 50 (1999) 207–225, https://doi.org/ 10.1016/S0920-5861(98)00504-5.
- [36] D. Haffad, A. Chambellan, J.C. Lavalley, Propan-2-ol transformation on simple metal oxides TiO₂, ZrO₂ and CeO₂, J. Mol. Catal. A Chem. 168 (2001) 153–164, https://doi.org/10.1016/S1381-1169(00)00516-1.
- [37] R.M. Ferrizz, G.S. Wong, T. Egami, J.M. Vohs, Structure sensitivity of the reaction of methanol on ceria, Langmuir 17 (2001) 2464–2470, https://doi.org/ 10.1021/la0017290.
- [38] D.R. Mullins, M.D. Robbins, J. Zhou, Adsorption and reaction of methanol on thin-film cerium oxide, Surf. Sci. 600 (2006) 1547–1558, https://doi.org/ 10.1016/j.susc.2006.02.011.
- [39] D.R. Mullins, S.D. Senanayake, T.-L. Chen, Adsorption and reaction of C1–C3 alcohols over CeOX (111) thin films, J. Phys. Chem. C 114 (2010) 17112–17119, https://doi.org/10.1021/jp103905e.
- [40] P.M. Albrecht, D.R. Mullins, Adsorption and reaction of methanol over CeO_x(100) thin films, Langmuir 29 (2013) 4559–4567, https://doi.org/ 10.1021/la400295f.
- [41] S. Rossignol, Y. Madier, D. Duprez, Preparation of zirconia-ceria materials by soft chemistry, Catal. Today 50 (1999) 261–270, https://doi.org/10.1016/ S0920-5861(98)00508-2.
- [42] A. Beste, S.H. Overbury, Pathways for ethanol dehydrogenation and dehydration catalyzed by ceria (111) and (100) surfaces, J. Phys. Chem. C 119 (2015) 2447–2455, https://doi.org/10.1021/jp509686f.
- [43] A. M, K.R. De Souza, G. Jacobs, U.M. Graham, B.H. Davis, L. V Mattos, F.B. Noronha, Applied Catalysis B: Environmental Steam and CO 2 reforming of ethanol over Rh/CeO2 catalyst, Appl. Catal. B Environ. 102 (2011) 94–109. https://doi.org/10.1016/j.apcatb.2010.11.030.
- [44] M. Nolan, J.E. Fearon, G.W. Watson, Oxygen vacancy formation and migration in ceria, Solid State Ion. 177 (2006) 3069–3074, https://doi.org/10.1016/j. ssi 2006 07 045
- [45] K. Hermansson, M. Baudin, M. Wo, Dynamics, structure and energetics of the (111), (011) and (001) surfaces of ceria, Surf. Sci. 468 (2000) 51–61.
- [46] M. Nolan, S. Grigoleit, D.C. Sayle, S.C. Parker, G.W. Watson, Density functional theory studies of the structure and electronic structure of pure and defective low index surfaces of ceria, Surf. Sci. 576 (2005) 217–229, https://doi.org/ 10.1016/j.susc.2004.12.016.
- [47] M. Fronzi, A. Soon, B. Delley, E. Traversa, C. Stampfl, Stability and morphology of cerium oxide surfaces in an oxidizing environment: A firstprinciples investigation, J. Chem. Phys. 131 (2009), https://doi.org/10.1063/ 1.3191784.

- [48] M. Nolan, S.C. Parker, G.W. Watson, The electronic structure of oxygen vacancy defects at the low index surfaces of ceria, Surf. Sci. 595 (2005) 223–232, https://doi.org/10.1016/j.susc.2005.08.015.
- [49] J.C. Conesa, Computer modeling of surfaces and defects on cerium dioxide, Surf. Sci. 339 (1995) 337–352.
- [50] T.X.T. Sayle, S. Parker, C.R.A. Catlow, The role of oxygen vacancies on ceria surfaces in the oxidation of carbon monoxide, Surf. Sci. 316 (1994) 329–336, https://doi.org/10.1016/0039-6028(94)91225-4.
- [51] J. El Fallah, S. Boujana, H. Dexpert, A. Kiennemann, J. Majerus, O. Touret, F. Villain, F. Le Normand, Z. Wu, M. Li, S.H. Overbury, C. Binet, M. Daturi, A. Badri, C. Binet, J. Saussey, J.-C.C. Lavalley, A. Bensalem, A. Badri, C. Binet, J.-C.C. Lavalley, Redox processes on pure ceria and on Rh/CeO₂ catalyst monitored by X-ray absorption (fast acquisition mode), J. Phys. Chem. 98 (1994) 6392–6398, https://doi.org/10.1016/S0920-5861(01)00415-1.
- [52] S. Bernal, J.J. Calvino, G.A. Cifredo, J.M. Gatica, J.A. Pérez Omil, J.M. Pintado, Hydrogen chemisorption on ceria: Influence of the oxide surface area and degree of reduction, J. Chem. Soc, Faraday Trans. 89 (1993) 3499–3505, https://doi.org/10.1039/FT9938903499.
- [53] A. Migani, G.N. Vayssilov, S.T. Bromley, F. Illas, K.M. Neyman, Dramatic reduction of the oxygen vacancy formation energy in ceria particles: A possible key to their remarkable reactivity at the nanoscale, J. Mater. Chem. 20 (2010) 10535–10546, https://doi.org/10.1039/c0jm01908a.
- [54] J.L.G. Fierro, J. Soria, J. Sanz, J.M. Rojo, Induced changes in ceria by thermal treatments under vacuum or hydrogen, J. Solid State Chem. 66 (1987) 154– 162, https://doi.org/10.1016/0022-4596(87)90230-1.
- [55] S.M. Schimming, G.S. Foo, O.D. Lamont, A.K. Rogers, M.M. Yung, A.D. D'Amico, C. Sievers, Kinetics of hydrogen activation on ceria-zirconia, J. Catal. 329 (2015) 335-347, https://doi.org/10.1016/j.jcat.2015.05.027.
- [56] A. Badri, C. Binet, J. Saussey, J. Lavalley, situ FT-IR study of ceria reduction by CO 699 (1997) 697–698.
- [57] J. Paier, C. Penschke, J. Sauer, Oxygen defects and surface chemistry of ceria: Quantum chemical studies compared to experiment, Chem. Rev. 113 (2013) 3949–3985, https://doi.org/10.1021/cr3004949.
- [58] D.R. Mullins, The surface chemistry of cerium oxide, Surf. Sci. Rep. 70 (2015) 42–85, https://doi.org/10.1016/j.surfrep.2014.12.001.
- [59] A. Siokou, R.M. Nix, Interaction of methanol with well-defined ceria surfaces: Reflection/absorption infrared spectroscopy, X-ray photoelectron spectroscopy, and temperature-programmed desorption study, J. Phys. Chem. B 103 (2002) 6984–6997, https://doi.org/10.1021/jp991127h.
- [60] T. Kropp, J. Paier, Reactions of methanol with pristine and defective ceria (111) surfaces: A comparison of density functionals, J. Phys. Chem. C 118 (2014) 23690–23700, https://doi.org/10.1021/jp505088b.
- [61] T. Prasomsri, M. Shetty, K. Murugappan, Y. Román-Leshkov, Insights into the catalytic activity and surface modification of MoO₃ during the hydrodeoxygenation of lignin-derived model compounds into aromatic hydrocarbons under low hydrogen pressures, Energy Environ. Sci. 7 (2014) 2660–2669, https://doi.org/10.1039/c4ee00890a.